PRODUCTION ENGINEERING ARCHIVES

ISSN 2353-5156 (print)
ISSN 2353-7779 (online)

Exist since 4th quarter 2013
Available online at https://pea-journal.eu

Root Cause Assessment of Welded Satellite Gear Carrier Failure in a Bucket Wheel Excavator

Dušan Arsić[1], Ružica Nikolić[2], Aleksandra Arsić[3], Dragan Cvetković[4], Otakar Bokuvka[2], Vesna Mandić[1]

[1] Faculty of Engineering, University of Kragujevac, Kragujevac, Serbia; dusan.arsic@fink.rs (DA); mandic@kg.ac.rs (VM)
[2] Research Centre, University of Žilina, Univerzitna 8215/1, 010 26 Žilina, Slovakia; ruzica.nikolic@uniza.sk (RN); otakar.bokuvka@fstroj.uniza.sk (OB)
[3] Faculty of Mechanical Engineering, University of Belgrade, Kraljice Marije 16, Belgrade, Serbia; aarsic@mas.bg.ac.rs
[4] Institute for Information Technologies, University of Kragujevac, Jovana Cvijića bb, Kragujevac, Serbia; dragan_cw8202@yahoo.com
*Correspondence: dusan.arsic@fink.rs

Article history
Received 20.05.2025
Accepted 27.03.2026
Available online 11.05.2026

Keywords
mining machinery;
structural integrity;
stress concentration;
finite element analysis;
vibration diagnostics;
low-cycle fatigue;
maintenance engineering.

Abstract
In this study was investigated the fracture of the welded supporting structure of a satellite carrier of a bucket wheel excavator drive reducer. The research was aimed at identifying the root causes of the failure through an integrated failure analysis combining theoretical calculations, numerical modelling and experimental investigations. The loading analysis included digging resistance, natural and forced oscillations of the excavator structure, and verification of the support strength under variable operating conditions. Finite element analysis was used to determine the stress state in the critical regions of the carrier, while the field measurements were performed to assess operational stresses and vibration behavior under different excavation regimes. In addition, metallographic and scanning electron microscopy examinations were carried out to identify the fracture features and weld imperfections. The results showed that the critical sections of the support structure operated under stresses close to the yield limit, while impact loads and low-frequency oscillations significantly increased the risk of failure. Fractographic observations revealed lamellar tearing, low-cycle fatigue features and a heterogeneous weld structure containing cracks, inclusions and gas porosity. The fracture was therefore caused by the combined effect of excessive service loads, dynamic excitation, stress concentration and imperfections in welded joints, which should be more comprehensively considered in the design and assessment of such structures.

DOI: 10.30657/pea.2026.32.19

1. Introduction

Bucket wheel excavators are subjected to a complex stress state arising from different phases of their structural and operational history. These stresses include residual stresses introduced during the fabrication and assembly, operational stresses generated under regular service conditions in response to static and dynamic loading, as well as non-stationary dynamic stresses associated with disturbed or transient operating regimes. The interaction of these stress components may significantly affect the structural integrity, particularly by promoting local stress concentration, damage accumulation, and the initiation and propagation of cracks in critical load-bearing components.

In addition, the influence of own low-frequency oscillations on the working strength of vital structures and parts cannot be fully understood in the design and construction phase (Arsić et al., 2019, a, b). The existing dynamic models of vital structures and parts, mechanisms and drives of rotary excavators, i.e., models of external load, caused by digging resistance, do not allow complex assessment of their influence on the dynamic behavior of rotary excavators as a whole (Arsić et al., 2025, Petrović et al., 2025).

In this article are presented partial results of the failure analysis of a fracture of the welded support structure of a satellite planetary gear of the BWE wheel drive.

Failure analysis (FA) is a multidisciplinary, multifaceted scientific field, connecting areas of engineering from diverse backgrounds and bodies of knowledge (Pantazopoulos, 2019).

The critical requirement in failure analysis is that it must be correctly conducted to provide all the necessary information that give substance to explanations for the root cause of the failure (Maisuradze and Antakov, 2021).

There are actually two types of articles dealing with application of failure analysis in engineering. The first group are articles devoted to using the FA to resolve concrete problems of some part/mechanism/device failure, while to the second group belong articles considering more general aspects of FA itself, with emphasis on its possible application to various types of failure problems. This short review of FA application articles contains only those directly related to the subject of this paper.

(Mohammed et al., 2012) were trying to identify the cause of failure of a connecting-rod shank in an engine, subjected to cyclic dynamic loading. The analysis included finite element calculations of the stress within the shank and metallographic investigation of the shank's fracture surface. The conclusion was that the fracture was caused by fatigue, and that the higher quality material-should be used for manufacturing the connecting-rod.

(Han et al., 2014) were investigating causes for the drill pipe fracture in Taho Oilfield in China, which fractured at depth of 1665.93 m, after 210.5 h of the service life. The results of FA showed that the failure of the drill pipe occurred due to the sulfide stress corrosion cracking (SCC) and that using the high strength steel was inadequate in the well that contains high amounts of the hydrogen sulfide.

(Zangeneh, Ketabchi and Kalaki, 2014) were investigating failure of an agitator shaft, made of the AISI 304L stainless steel, in a large vessel. They have shown that while the mechanical properties and chemical composition of the failed shaft material were within the acceptable range, the existence of a single machining groove of a depth of 0.2 mm caused the stress increase for as much as 50 %. Thus, the inadequate fillet radius size and machining grooves on the shaft surface were the main causes of its failure.

(Gong, Ding and Yang, 2019) were trying to discover what caused the premature fracture during service of three of the four TP321 stainless steel anchor bolts used in an indoor seawater booster pump of a nuclear power plant. The FA conclusion was that the premature fractures were caused by the stress corrosion cracking (SCC) from chlorides, which occurred due to splashing of the seawater during the routine maintenance of the pump.

(Katinic et al., 2019) were analyzing the cause of the corrosion fatigue failure of the steam turbine rotor's moving blades, of a condensing industrial steam turbine installed in a fertilizer production plant. Authors proposed measures to extend the service fatigue life of the rotor blades, by redesigning the whole turbine stage that increased the fatigue safety factor by about 50 %.

(Krishnakumar and Selvakumar, 2020) conducted a metallurgical investigation of failed bearing and chain parts, through the chemical analysis, optical metallography and hardness analysis. The impact fatigue was the cause of fractures, as well as overload and unsuitable material selection.

(Husaini, Putra and Novriandika, 2020) studied the fracture of the crankshaft pulley used on a truck engine, by visual examination, chemical and SEM analysis, as well as using the finite element analysis (FEA) to quantify the stress intensity factor (SIF) distribution near the crack tip in the crankshaft pulley. The reason for the crack initiation was the stress concentration in the sharp-angled keyway.

(Maisuradze and Antakov, 2021) presented an analysis of failures of mechanical components made from alloyed steels, and identified fatigue cracking, and flaws in thermal, thermochemical and mechanical treatments as causes of those failures.

(Bakhshandi et al. 2022) tried to explain the failure mechanisms of two cylindrical impact pistons, made of two different steel grades, subjected to impact loading. The results have shown that the failure of both pistons started with degradation of the impact surfaces, as cavitation erosion and localized surface fatigue phenomena, followed by chipping and removal of material from impact surfaces.

(Rocha Pinho, Campanelli and Pereira Reis, 2022) were conducting a failure analysis to discover the cause of fracture of the turbojet compressor blades, which occurred during the laboratory tests. The visual and fractographic analyses pointed to the fact that the turbojet compressor failed due to fatigue as a consequence of the surface roughness, especially in the transition from the body to the blades, which acted as a stress concentrator causing the cracks nucleation on the blades' surfaces.

(Sulaiman and Abidin Ismail 2013) tried to interpret the machine failure in a suitable manner. They discussed application of the two methods of FA, the so-called Why-why analysis and the PM analysis. The Why-why analysis consists of chain of questions. The first answer should be the direct cause of a certain part/assembly failure. When the root cause of failure is identified that would be the point to stop asking Why. The PM (phenomenon-mechanisms) analysis consists of identifying the 5 Ms of FA: mechanisms /machinery/men/ materials /methods.

(Kaulgud and NangarePatil, 2016) have dealt with different types of material and component failures that appeared in industrial enterprises. They emphasized the critical importance of fractography for failure analysis of metals and plastics, pointing to the fact that fractography of plastics is a relatively new field, though bearing many similarities to metals' behavior.

(Pantazopoulos, 2019) presented a review on fracture mechanisms of mechanical components operating under industrial process conditions, with emphasis on the phenomenological aspects of fracture and their relationships with the emergent fracture mode(s), taking into account the prevailed operating parameters and loading conditions.

(Guma, Ozoekwe and Odita, 2020) conducted an overview of approaches and techniques used in failure analysis of engineering system, presenting 24 recent works of researchers from different backgrounds. They emphasized that "although there are many existing FA approaches and techniques of engineering systems, not all, or a number of them, can be suitable for every particular failure case".

(Espinel-Blanco et al., 2021) proposed a two-stage method for fault analysis in metal materials that have failed due to fracture. The first stage would consist of a visual inspection of the failed element, while the second stage would assume a series of destructive tests to identify the characteristics of the material and the occurrence of the failure.

(Fathyunes and Mohtabi-Bonab, 2023) conducted a review on the corrosion and fatigue failure of gas turbines, declaring that one of the main causes of failure in turbines is corrosion fatigue, which is a result of combined action of cyclic loads and corrosive environment. They also presented a summary of the literature results related to influence of the loading conditions, corrosive environment and properties of the turbine materials on this failure.

Similar researches were conducted by (Vulović, 2023, Arsić et al., 2019 b and Zhao, 2017).

(Dudzinski et al., 2024; 2025) conducted analysis of the discharge boom suspension axle failure, which caused uncontrolled movement of the discharge boom. The results pointed to the fact that the fracture was caused by material fatigue, as a combination of three factors: inappropriate material microstructure, notch effect and cyclic loading. The nominal design loads were lower for 18% than the measured ones, which was the additional factor that contributed the failure of the axle.

(Song et al., 2025) have investigated the failure of a 750A dual-insulated pipeline, where the cracks have developed along the weld joints during the heat supply resumption at the district heating facility. The analysis included the visual inspection, mechanical testing, microstructural characterization, finite element analysis (FEA), and electrochemical corrosion testing. The results indicated that cracks were generated in the heat-affected zone (HAZ), primarily caused by galvanic corrosion and thermal expansion-induced stress accumulation. Finite element analysis showed that the stresses in the Coarse Grain HAZ surpassed the yield strength of both the base metal (349 MPa) and weld metal (384 MPa) and the peak value was 475 MPa.

Thus, the general conclusion is that in the FA it is always necessary to select the best approach and technique, suitable for analysis of each particular failure of a part or a system, and, if possible, present those even before the eventual failure.

On the other hand, methods for detecting the construction errors have evolved and are constantly being improved. Apart from the classic ones that are still widely used (Arsić et al., 2021), there are also newer methods that can provide greater precision in work or even indicate a problem with the construction in exploitation earlier.

Bucket Wheel Excavators (BWEs) are among the largest and most critical assets in continuous surface mining. Their welded structures, such as the boom, bucket wheel, and supporting frames, are subjected to extreme cyclic and dynamic loads, leading to complex failure mechanisms like fatigue, brittle fracture, and stress-corrosion cracking. Traditional visual inspection and basic non-destructive testing (NDT) are often insufficient for predicting failures. The latest global diagnosis paradigm integrates advanced NDT, numerical modelling, and structural health monitoring (SHM) to enable predictive and proactive failure analysis.

Phased Array Ultrasonic Testing (PAUT) represents the technique that offers superior detection and sizing of internal weld defects like lack of fusion, cracks, and porosity. Its ability to electronically steer and focus beams provides detailed cross-sectional images of the weld, which is crucial for assessing the crack propagation in thick BWE components (Sampath et al., 2021).

Digital Radiography (DR) is replacing traditional film radiography. The DR provides immediate, high-resolution images of weld integrity with enhanced sensitivity. It is particularly effective for inspecting the complex weld geometries in the bucket wheel hub and boom connections.

Acoustic Emission (AE) Testing is a passive, global monitoring technique that detects the high-frequency stress waves released by active defects (e.g., growing cracks) under load. Its major advantage for BWEs is the ability to monitor large structures in real-time during operation, pinpointing active damage zones before they become critical (Barski and Płachta, 2013). Recent work by (Świt et al., 2024) further confirms that acoustic emission can support the monitoring of crack development and the assessment of structural integrity in steel components, although in a different application domain.

One of the newer inspection methods in engineering today is Structural Health Monitoring (SHM) with Fiber Optic Sensors. That technique represents a shift from periodic inspection to continuous monitoring. Fiber Bragg Grating (FBG) sensors are at the forefront of this shift. They are embedded or surface-mounted on critical welds to provide the real-time, in-situ strain and temperature data. Their immunity to electromagnetic interference, small size, and ability to be multiplexed in a single fiber line make them ideal for the extensive and electrically noisy environment of a BWE. This allows for the direct measurement of operational stresses and the detection of abnormal load patterns that precede failure (Michałek et al., 2019).

Besides the experimental testing on these systems, Numerical Simulation and Digital Twins are using the wider possibilities today, compared to the earlier times. The Finite Element Analysis (FEA) is no longer used just for design but is integral to failure diagnostics. By creating a high-fidelity digital model of the BWE's welded structure, engineers can simulate load scenarios and identify the potential high-stress concentration zones (hot-spots) prone to fatigue cracking. The latest evolution is the concept of a Digital Twin, where the FEA model is continuously updated with real-world operational data from SHM sensors. This creates a live, virtual replica of the physical asset, enabling predictive analysis of remaining fatigue life and accurate diagnosis of the root cause of failures (Heinrich, 2022).

Apart from the mentioned techniques, the Integrated Approach for BWE Assemblies can today be considered as one of the most effective diagnostic strategies. For instance, an AE system can provide a global warning of active cracking in a boom structure. This warning then triggers a targeted, high-resolution PAUT inspection to precisely characterize the detected flaw. Subsequently, an FEA model, calibrated with strain data from the FBG sensors, is used to assess the criticality of the flaw and predict its growth rate under future loading

cycles, thereby informing about the optimal repair decisions and preventing the catastrophic downtime.

2. Analysis of the support structure parts loads

In this paper is presented a methodological approach to the failure analysis of the cause of a fracture of the welded structure of the satellite carrier of the planetary part of the reducer for driving the excavator rotor.

The excavator SRs 1300.26/5.0+VR±10, produced by "TAKRAF", Germany, is shown in Fig. 1, the cross-section of the reducer in Fig. 2, and the elements of the satellite carrier of the planetary part of the drive reducer in Fig. 3 (TAKRAF SRs 1300.26/5.0+VR±10, Equipment manufacturer's documentation).

Fig. 1. Rotary excavator SRs 1300.26/5.0+VR±10

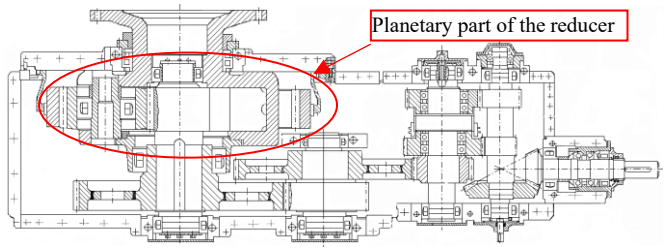

Fig. 2. The cross-section of the drive reducer of the working wheel

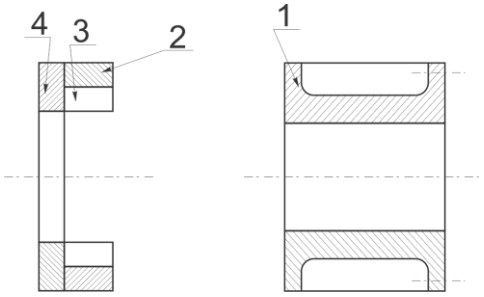

Fig. 3. Elements of the satellite carrier of the planetary part of the drive reducer of the rotor excavator: 1 – the upper flange, 2 – the reinforcing rib, 3 – the drive plate, 4 – the segment

The construction solution of the reducer with a planetary part at the output enables the rotor speed to be 7.108 rpm or 5.787.

According to the documentation received from the equipment supplier, the elements of the satellite carrier of the planetary part of the drive reducer of the excavator rotor are made of the following materials: the upper flange (1) is made of the cast steel GS-E 50.3, the reinforcing rib (2) and the drive plate (3) are made of steel 38B2 and the segment (4) is made of sheet steel S355JR.

The welding of parts of the satellite carrier, according to the equipment supplier, was performed using procedures 111 (EN ISO 4063: Welding processes 111) and 135 (EN ISO 4063: Welding processes 135). Additional material is 10 MnSi, preheating temperature 150 °C, heat treatment - annealing at a temperature of 500 - 550 °C and the non-destructive testing was carried out using the magnetic particle method. The intended quality class of the welded joints is "B" (EN ISO 5817).

The basic technical characteristics of the rotor excavator reducer are given in Table 1.

Table 1. Technical properties of the rotor excavator reducer

Property	Value
The highest transmission ratio	i = 249.7
Number of the electric motor revolutions	n = 1485
Output power	P = 900 kW
Voltage	U = 6000 V
cos α	0.88
Output torque in excavator operation	T_{ow} = 1374 kNm
Output torque when starting the excavator	T_{os} = 1786 kNm

2.1. Digging resistances

During exploitation, most assemblies and elements of the rotary excavator are exposed to complex dynamic loads, which depend on the conditions of exploitation, i.e., digging resistance and self-oscillations, in stationary and non-stationary operating modes of the excavator drive system.

Determining the external load on the excavator rotor from digging resistance appears as a basic need both during the design and exploitation. Numerous parameters, which define the resistance in the process of digging with a rotary excavator, are classified into three groups: rock mass parameters, geometric parameters of digging and structural-kinetic characteristics of the excavator.

The rotor of an excavator with buckets needs to overcome the resistance of cutting, lifting the excavated material, filling the bucket, friction of the soil material and friction between the material and the bucket, which depend on the cutting parameters and the characteristics of the working environment. In practice, it is necessary to determine the total resistances, because they are decisive for the correct selection and sizing of the rotary excavator, Figure 4.

The basic component of the digging resistance is the tangential component F_t, kN, defined as the product of the specific linear digging resistance along the knife length k_L, kN/m and the sum of the average lengths of the cutting edges of the knives in the engagement L_{av}, m, or the specific surface digging resistance of the cross-sectional area of the chops k_A, kN/m^2 and the sum of the average cross-sectional areas of the chops A_{av}, m^2, depending on the number of buckets z on the rotor and the angle digging φ, °:

$$F_t = \begin{Bmatrix} k_L \cdot L_{sr}; L_{sr} = \dfrac{z}{2\pi} \cdot \int^{\phi\alpha} L(\phi) d\phi \\ k_A \cdot A_{sr}; A_{sr} = \dfrac{z}{2\pi} \cdot \int^{\phi\alpha} L(\phi) d\phi \end{Bmatrix} \quad (1)$$

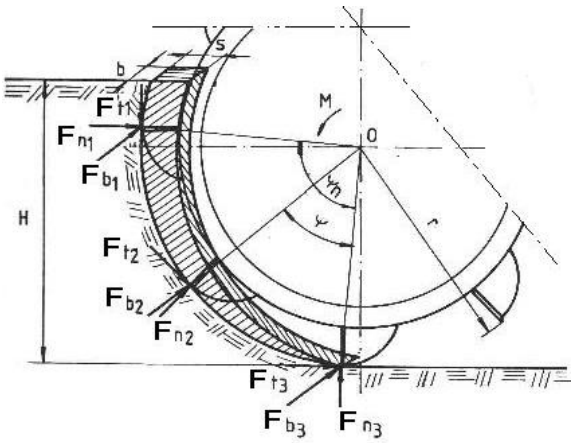

Fig. 4. Digging resistances for the rotary excavator SRs 1300.26/5.0+VR±10

The total digging resistance F_d represents the spatial load, which consists of three components: tangential F_t, normal due to the rotation of the rotor F_n, and lateral due to the circular movement of the excavator superstructure with the working wheel and boom F_s:

$$F_d = \sqrt{F_t^2 + F_n^2 + F_s^2}\,, \quad (2)$$

where:

$$F_n = \psi_n \cdot F_t \quad (3)$$

and

$$F_s = \psi_s \cdot F_t\,. \quad (4)$$

The nominal digging power N, kW, which depends on the efficiency ratio of the drive electric motors η, can be defined as the sum of the power required for digging N_d and the power required for lifting and loading the excavated material N_h:

$$N = \frac{1}{\eta} \cdot (N_d + N_h)\,. \quad (5)$$

Based on the characteristics of the digging resistance of one bucket, as a random function of the digging angle, it is possible to proceed to the statistical characteristics of the total load of the rotor, i.e., the rotor shaft $F(\varphi)$ and the torque on the rotor shaft $T(\varphi)$. Variables $F(\varphi)$ and $T(\varphi)$ are used for dimensioning drive systems. Their exact values are obtained by measurements on a large number of buckets, on a large number of rotary excavators, and for a number of different excavation environments.

2.2. Excavator natural and forced oscillations

The connection of the upper rotating and moving part of the rotary excavator represents, in comparison to the rotor boom, loading boom and counterweight, a small basis for the stability of the structure in operation. Due to that, the excavator is relatively easily brought into a state of oscillation, both in stationary and non-stationary modes of operation, whereby the induced oscillations of vital structures lead to dynamic stresses in the structural elements. Excavator oscillations can be complex and have a wide frequency spectrum.

Oscillations of the vital structures of the rotary excavator are characterized by translational and/or rotational movement of the intersection points, i.e., their distance from the neutral position, which changes in time.

Based on the manufacturer's technical documentation and the dimensions of the construction elements of the rotor boom, the calculation of the forces in the rods and the displacement of the nodes of the spatial grid, as well as the calculation of the masses and stiffness coefficients for individual rods, was performed.

In addition, the natural vertical oscillations of the boom were calculated using the "Finite-storelemente" method, for the plane lattice model, Fig. 5. When calculating the frequency of natural oscillations, it was assumed that the masses as rigid elements are concentrated in the nodes, and that the elastic elements are placed in the convergent directions of the rods of the lattice model. Based on the displacement of the mass of each rod and each node, the total mass of the lattice was determined.

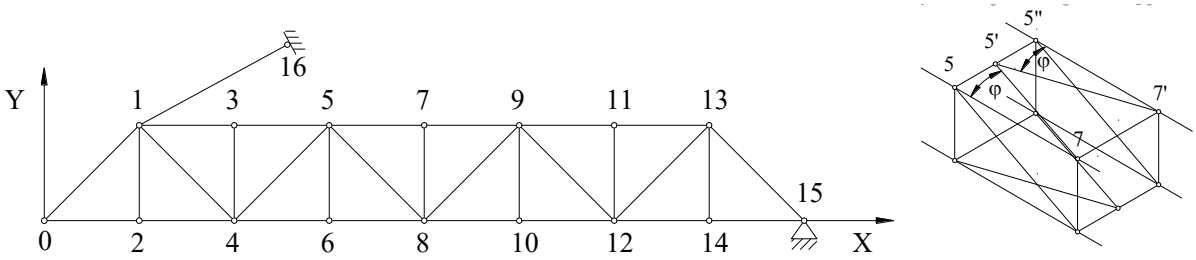

Fig. 5. Calculation model of the rotor boom for vertical oscillations

The calculated approximate values of natural oscillation frequencies for the approximate model of the rotor boom grid are: f_{min} = 4.58, Hz and f_{max} = 195.0, Hz.

2.3. Calculation of the satellite support strength

The satellite carrier in the planetary section of the reducer driving the excavator bucket wheel is subjected to the driving torque and transverse bending forces. To evaluate its mechan-

ical response, a theoretical analysis of the stress state was performed under different loading conditions. A comparable approach to load determination in load-bearing rotary components, with particular emphasis on actual support conditions and stiffness effects, was reported by (Krynke et al., 2023). The analysis considered the following load cases:
• Case 1, loading of the satellite carrier caused by rotational force,
• Case 2, loading of the satellite carrier caused by its self-weight and alternating bending,
• Case 3, satellite carrier loads caused by alternating bending.

The conducted research was aimed at checking the safety of the satellite carrier according to the yield strength and fatigue strength.

The driving torque load is transmitted through the bearing on the satellite carrier plate. For the ideally distributed load.

The force in the bearing of the planetary gear that acts along the perimeter, is calculated as:

$$F_D = \frac{M_{Ab}}{D_p \cdot a_p}, \tag{6}$$

where: M_{Ab} is the driving torques, D_p is the bearing diameter and a_p is the numberer of the planetary gears.

The satellite carrier is loaded with the driving circumferential force and the bearing forces in the housing, Fig. 6.

Data for calculations are given in Table 2.

Static calculation under the action of the same nominal loads gives the bearing force in the housing $F_{NU} = 2.34 \cdot 10^5$, N. At the double nominal load, i.e., in the case when coupling torque is also taken into account $F_{CU} = 3.73 \cdot 10^5$, N.

Table *2.* Data on loading and planetary gear dimensions

Forces, kN		Dimensions/lengths, m								
F_G	F_u	b_C	b_G	b_u	a	b	a_G	l_1	l_2	l_3
260	332	0.59	0.58	0.97	8.566	1.165	1.6	0.203	0.466	1.08

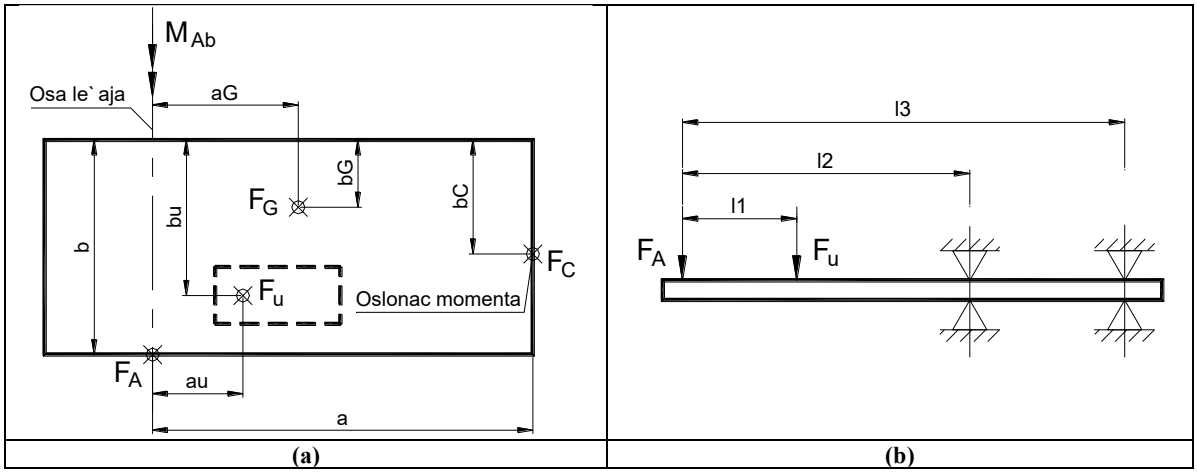

Fig. 6. (a) Gear box load display (top view); **(b)** Positioning and loading of the planetary shaft of the drive gear

2.4. Calculation of the support structure fatigue strength

The calculation of the fatigue strength of the upper flange (1) and segment (4) of the welded satellite support was performed based on the predicted (calculated) normal distribution load spectra (Savković et al., 2011)]. The stress of the satellite support is determined based on the digging resistance, oscillation of the structure during the digging process and circular bending by transverse forces. The stress components are: σ_{MN} - comparative stress due to torsion moment, σ_{QN} - comparative stress due to transverse stress caused by torque,
σ_{QG} - comparative stress due to own weight and σ_N - comparative effective stress at the most loaded places. The calculated values of stress components are given in Table 3.

Table 3. Calculated stresses of the most loaded places of the satellite carrier parts, N/mm^2

Part	σ_{MN}	σ_{QN}	σ_{QG}	σ_N
Flange	95.2	13.7	9.3	118.2
Drive plate	94.7	8.3	5.7	108.7

2.5. Numerical calculations of stresses and deformation

The stress and deformation analysis of the planetary carrier of the satellite was carried out by numerical calculation, using the finite element method and the hemisphere program of the AUTRA system (owned by the mine where the excavator was in operation). In Fig. 7 is presented the mesh model for 1/4 of the satellite carrier and in Fig. 8 calculation models of the satellite carrier loads.

The comparative stresses σ_c were calculated according to:

$$\sigma_c = \sqrt{\sigma^2{}_x + \sigma^2{}_y - \sigma_x \cdot \sigma_y + 3 \cdot \sigma^2{}_{xy}}\ , \tag{7}$$

where: σ_x and σ_y are the normal stress components and σ_{xy} is the shear stress.

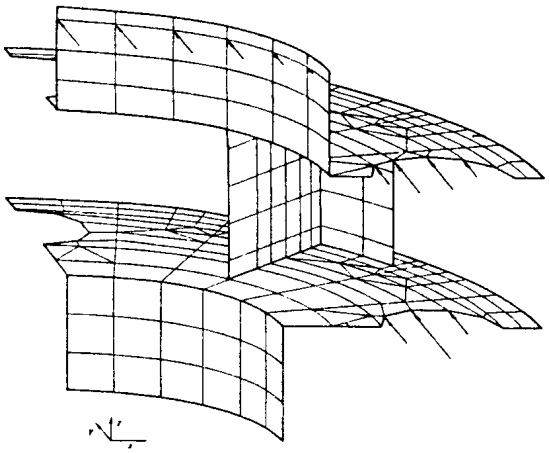

Fig. 7. The support structure mesh model

2.6. Safety checking for exceeding the yield stress

Given that the AUTRA program enables the calculation of maximum spatial stresses, the procedure was applied for the calculation of safety related to the plastic yield strength. It allows for the possibility that the yield stress may be exceeded in the most stressed part of the structure, without visible deformations of the structure, provided that the remaining deformation due to tension is $e_R = 0.002$. For the required condition, the safety coefficients were calculated using the data from Table 4, according to:

$$S_y = \frac{\delta_{0.2} \cdot \sigma_c}{\sigma_{c\max}}\ , \tag{8}$$

where: $\delta_{0.2}$ is the ratio for the yield stress for the circular ring plate, under the same yielding conditions; σ_c is the calculated comparative stress for the given mesh model and σ_{cmax} is the maximum comparative stress at macro elements.

Table 4. Calculated safety coefficients

Part	σ_c N/mm^2	σ_{max} N/mm^2	$\delta_{0.2}$	S_y
Front plate of the satellite carrier	235	211	1.8	2.00
Back plate of the satellite carrier	260	225.5	1.75	2.02

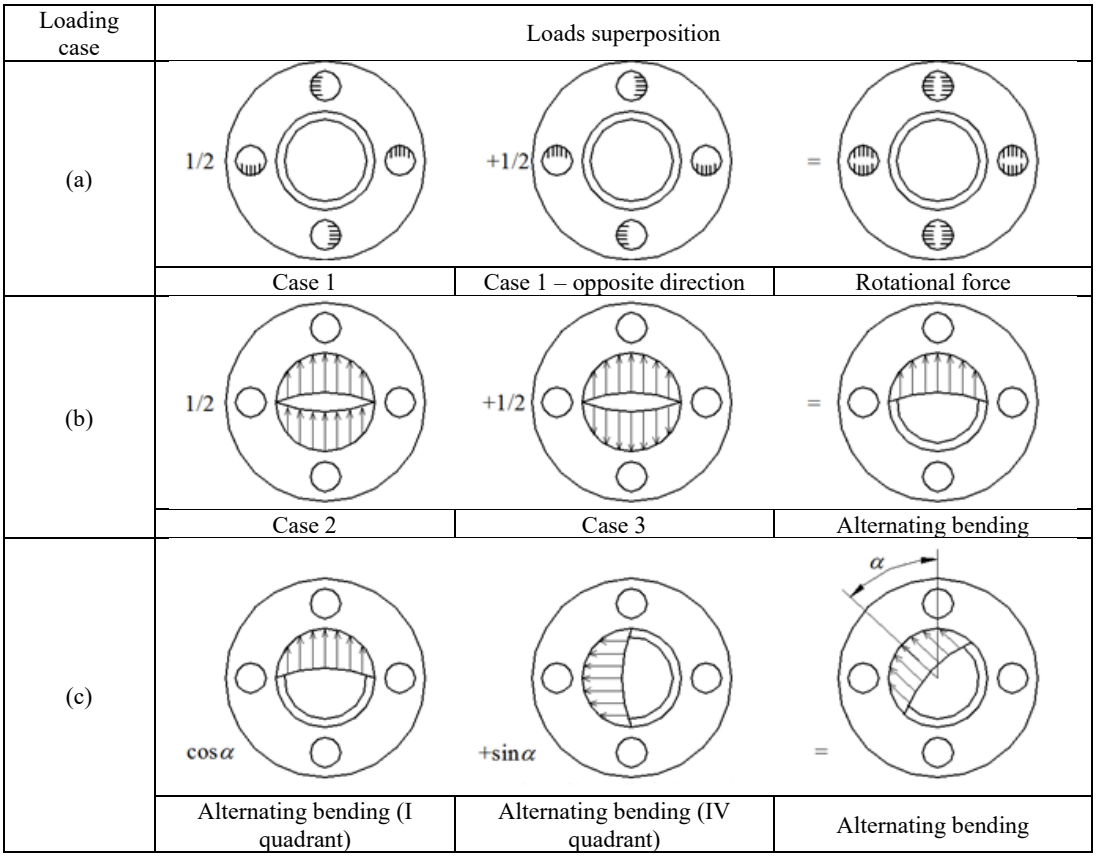

Fig. 8. Computational model of the load on the satellite carrier Computational model of satellite carrier load, superposition of loads due to: **(a**) rotational force; **(b)** own weight and alternate bending; **(c)** alternate bending

3. Experimental investigation

Experimental tests of digging resistance, natural and forced oscillations and deformation measurements to define the stress spectrum were performed on a rotary excavator of the same type, under operating loads in different excavation environments. The testing machine had all the important characteristics (nominal strength, wight, dimensions, digging equipment and the complete driving mechanism) identical to the excavator on which the broken part was operating.

Digging resistances were determined based on the measurement of the engaged power, which was performed by measuring the change in current strength at the working loads of the rotary excavator for certain phases of operation in different excavation environments.

For the maximum measured loads and total measurements, the parameters of the normal distribution law of the specific digging resistance k_L were calculated. For the maximum measured loads, the mean value is 86.3, kN/m with a standard deviation of 23.2, kN/m, and for the total loads the mean value is 68.2, kN/m with a standard deviation of 23.2, kN/m. It was found that checking the extreme values for $\pm 3\sigma$ is satisfactory.

To examine the natural and forced oscillations of the rotor boom structure, measurements of vertical and horizontal displacements and velocities and accelerations were made, in different load regimes and in hard-to-work environments, when strong impact loads occur. Measurements were made in the middle of the supporting vertical columns and in the middle of the main supports of the upper belt of the rotor boom, using the vibration method using a noise and vibration analyzer.

The application of vibration-based diagnostics in the present study is in line with (Biały 2024), who demonstrated that such methods can effectively support the assessment of degradation and technical condition of mining machinery under operating conditions. The values of the fundamental frequencies of self-oscillations, determined by analysis of oscillations during the transport and working movements of the excavator outside the digging process, are: vertical oscillations 1.0 - 3.2, Hz; transverse oscillations 0.5 - 0.7, Hz and longitudinal oscillations 0.4 - 0.5, Hz.

It was also determined that the logarithmic decrement of damping is $p = 0.5$, which represents a relatively small damping power and indicates the possibility of resonance.

The largest vertical oscillations in the operation of the excavator were recorded on the main supports of the rotor boom in the frequency analysis area of 2.5 - 5.0, Hz. This confirms that the danger of oscillation exists in the low-frequency area, as well.

Tensometric measurements of deformations were performed with four measuring tapes of type XY-120-HBM, which are suitable for measuring deformations caused by torque. Obtained values of the maximum established stresses for different load regimes are shown in Table 5.

Table 5. Maximum established stresses for different load regimes

Simulated excavator operation mode	Measured stress, MPa
Rotor start-up	110
Load when working in loose material	110
Average load (mixed layer of excavated mass)	140
Working in compact gray clay	160
Impact loads	220
Rotor start-up	110

4. Analysis of the satellite support fracture surfaces

Metallographic examinations of the fracture surfaces of the material samples of the satellite carrier parts revealed a ferrite-pearlite structure, which corresponds to the basic materials.

Based on a visual inspection of the fracture surface of the satellite carrier flange and analysis of the propagation of cracks, the lamellar separation of the material was determined, Figure 9. The lamellar cracks start from the base material or heat-affected zones. They are of the stepwise shape and parallel to the surface of the flange, and are the result of the welding technology, the action of stress in the direction of the thickness of the base material, depending on the properties of the base material (due to the thermal cycle of welding) and the structural solution of the welded joint. The appearance of the satellite carrier flange fracture surface with indicated a part of low-cycle fatigue is shown in Figure 10. This interpretation is consistent with fracture-mechanics studies showing that crack-front evolution and propagation in constrained structural regions may be strongly affected by local geometric and material discontinuities (Djoković et al., 2023).

Scanning electron microscope revealed that the weld metal has a very heterogeneous structure with a large number of defects (bonding faults, cracks, inclusions, gas bubbles), Figures 11-13.

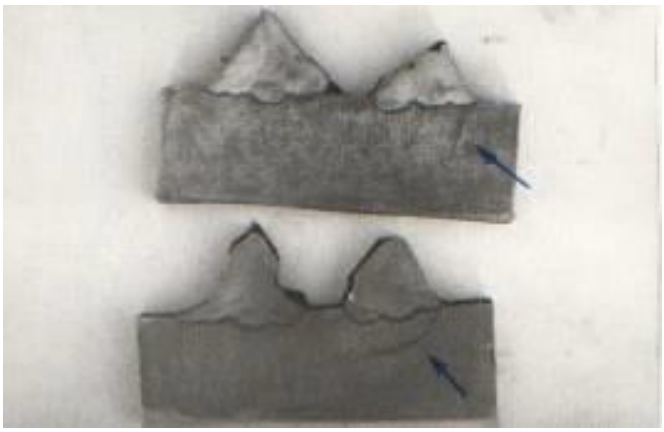

Fig. 9. The lamellar material separation of the upper flange of the satellite carrier

Fig. 10. The fracture surface of satellite carrier flange with indicated low-cycle fatigue (blue arrow)

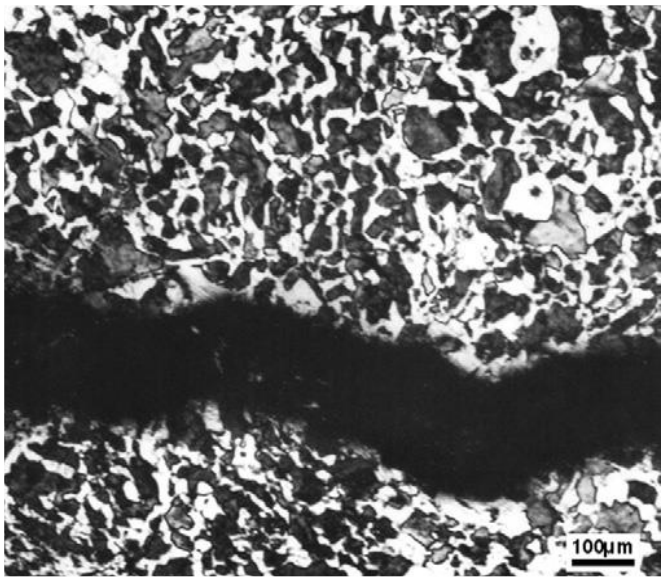

Fig. 11. The crack in the weld metal

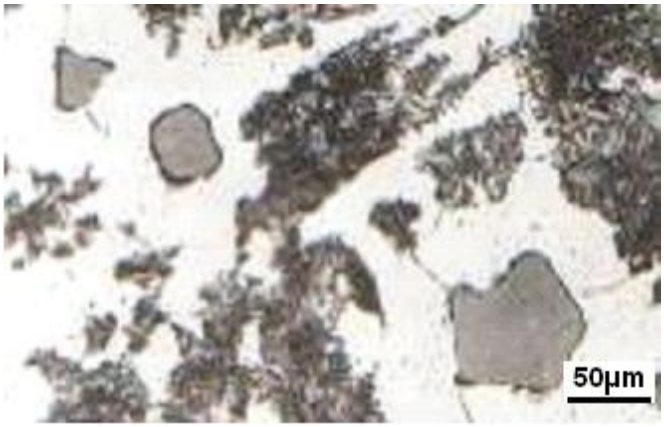

Fig. 12. The inclusions in weld metal

Fig. 13. The gas bubbles in the weld metal

5. Conclusions

The process of designing and developing the structure of the reducer for driving the excavator rotor is always accompanied by the prediction of its safety in operation and the prediction of the service life.

The analysis of the measurement results of the load (stresses), for different modes of excavator work, depending on the realized hourly production and statistical characteristics of the specific digging resistance, showed that the technical-technological characteristics fully meet the requirements when the excavator works on the excavation of transition zones between the two blocks of gray clay and in loose zones, but it does not satisfy the conditions of the excavator on the excavation of compact gray clay, due to significant shock loads in the work of the excavator, causing low-frequency oscillations.

The rotary connection of the upper rotating and moving part of the excavator represents, compared to the working boom and the balance boom with a weight, a relatively small basis for the stable operation of the structure in the area of low-frequency oscillations, where there is a danger that the frequency of its own oscillations will be close to the frequencies of oscillations caused by the periodic action of an external load, which can lead to the appearance of resonance and the failure of the most stressed sections.

By comparing the stresses determined by theoretical considerations and experimental tests, in relation to the carrying capacity of the satellite carrier, it was determined that the working stresses in the critical sections are close to the yield point and without taking into account the stress concentration.

The structural solution of the elements of the satellite carrier and the results of the experimental tests of the basic materials and welded joints showed that during the design and production of the welded structure, i.e., welded joints, as critical points, not all the parameters that are important in variable load conditions, are included. In the case of welded joints, there is an influence and concentration of stress, not only from the change of geometric shape, but from the errors present in the welded joints, as well, some of which remain in the construction even before it is being put into operation.

To achieve the required power and achieve the expected service life of the reducer, it is necessary to have accurate data on the load of the reducer for different operating modes in various excavation environments, already in the design phase. In addition, considering that welded joints belong to the critical places of the structure; by studying the behavior of materials and welded joints under the effect of variable load, data should be obtained that would help to realize a construction that is safe in relation to impact loads and fatigue failure.

Techno-economic justification of maintenance operations can be established using several decision-support approaches, including the Economic Method (MEC), Profitability Improvement Analysis (PIA), the Machinery and Allied Parts Institute Method (MAPI), and the Net Present Value Method (MNPV) (Mutavdžić, 2015; Lazić et al., 2014). These methods provide a structured analytical basis for selecting the optimal maintenance strategy by incorporating criteria related to economic feasibility, repair effectiveness, technological applicability, and the expected service performance of the restored system. Their application should cover failure analysis, evaluation of repair technologies for damaged components, and, where technically and economically justified, replacement with newly manufactured parts. The same criteria may also be extended to the assessment of alternative manufacturing technologies intended for new working elements, particularly when the long-term operational reliability and cost efficiency are considered. In practice, the preferred option is selected through the comparative evaluation of technological alternatives against profitability-related indicators, while accounting for both the range of available technical solutions and the limitations imposed by available financial resources. Investment appraisal is therefore typically based on measures of relative profitability, absolute economic return, and the anticipated benefits associated with improved operational effectiveness and reduced maintenance-related losses.

For conducting the failure analysis of the considered fractured part, the question was not whether to repair it or purchase the new one. The latter alternative was not an option due to the extremely high costs; thus, the former was adopted. On the other hand, this whole analysis has shown that the study of the behavior of a structure with welded joints must include a significantly larger number of parameters than required when studying the steel in the form of plates, since the heterogeneity of the structure of a welded joint is determined by different behavior of the base material, the heat-affected zone and the weld metal under the effect of variable loads. This conclusion is consistent with the findings of (Ivković et al., 2023), who showed that for responsible welded assemblies, the selection or substitution of steel must be preceded by verification of mechanical properties, weldability, and welding technology in order to ensure reliable structural performance under service loading.

Acknowledgements

The research, results of which are presented in this article, was partially financially supported within the project “Support of research and development capacities to generate advanced software tools designed to increase the resilience of economic entities against excessive volatility of the energy commodity market”, of Operational Programme Integrated Infrastructure, number ITMS2014+ code 313011BUK9, co-funded by the European Regional Development Fund and by the Faculty of Engineering, University of Kragujevac, Serbia through funds provided by the Ministry of Science, Technological Development and Innovation, Republic of Serbia, Agreement No. 451-03-34/2026-03/200107 - The research presented is in line with Sustainable Development Goals 9: Industry, Innovation, and Infrastructure, and 12: Responsible Consumption and Production.

References

Arsić, D., Gnjatović, N., Sedmak, S., Arsić, A., Uhričik, M., 2019(a). Integrity assessment and determination of residual fatigue life of vital parts of bucket-wheel excavator operating under dynamic loads, Engineering Failure Analysis, 105, 182-195, DOI: 10.1016/j.engfailanal.2019.06.072

Arsić, D., Nikolić, R., Arsić, A., Cvetković, D., Pastorkova, J., Bokuvka, O., 2025. Measures to prevent damage and to extent the service life of a rotary excavator, Production Engineering Archives, 31(1), 73-80, DOI: 10.30657/pea.2025.31.7.21

Arsić, D., Nikolić, R., Lazić, V., Arsić, A., Savić, Z., Djačić, S., Hadzima, B., 2019(b). Analysis of the cause of the girth gear tooth fracture occurrence at the bucket wheel excavator, Transportation Research Procedia, 40, 413-418, DOI: 10.1016/j.trpro.2019.07.060, 2019

Arsić, M., Arsić, D., Flajs, Ž., Grbović, A., Todić, A., 2021. Application of non-destructive testing for condition analysis, repair of damages and integrity assessment of vital steel structures, Russian Journal of Nondestructive Testing, 57(10), 918-931, DOI: 10.1134/S1061830921100053, 2021

Bakhshandi, R.K., Tkachuk, A., Sadek, M., Bergström, J., Grehk, M. 2022. Failure analysis of two cylindrical impact pistons subjected to high velocity impacts in drilling applications, Engineering Failure Analysis, 140, 106623. DOI: 10.1016/j.engfailanal.2022.106623

Barski, M., Płachta, A., 2013. Diagnostics of the supporting structure of a bucket wheel excavator using acoustic emission method. Key Engineering Materials, 569-570, 978-985

Biały, W. (2024). Assessment of the technical state of mining machinery and devices with the use of diagnostic methods. Production Engineering Archives, 30(2), 266–272. DOI: 10.30657/pea.2024.30.26

Djoković, J. M., Nikolić, R. R., Pastorková, J., Ulewicz, R. (2023). Prediction of the crack front shape of the corner interface crack. Applied Sciences, 13(23), 12584. DOI: 10.3390/app132312584

Dudziński, W., Odyjas, P., Olejnik, M., Moczko, P., Pietrusiak, D., Więckowski, J., 2025. Root cause analysis and evaluation of corrective actions for discharge boom suspension failure in bucket wheel excavator, Scientific Reports, 15, 28384, DOI: 10.1038/s41598-025-13312-9.

Dudziński, W., Moczko, P., Odyjas, P., Olejnik, M., Pietrusiak, D., Więckowski, J. 2024. Design examination, failure analysis and repair of the discharge boom suspension of the bucket wheel excavator. Procedia Structural Integrity, 58, 54-60, DOI: 10.1016/j.prostr.2024.05.010.

EN ISO 4063: Welding processes 111: Manual metal arc welding or stick welding, Welding and allied processes, Nomenclature of processes and reference numbers, European Committee for Standardization; 2010.

EN ISO 4063: Welding processes 135: Metal active gas welding, Nomenclature of processes and reference numbers, European Committee for Standardization; 2010.

EN ISO 5817: Welding - Fusion-welded joints in steel, nickel, titanium and their alloys (beam welding excluded) - Quality levels for imperfections, 2007.

Espinel-Blanco, E., Perez-Rangel, N.Y., Florez-Solano, E. 2021. Fracture failure analysis of metal materials by visual inspection and destructive testing. Journal of Physics Conference Series 2046(1):012060, DOI: 10.1088/1742-6596/2046/1/012060

Fathyunes, L., Mohtadi-Bonab, M.A. 2023. A Review on the Corrosion and Fatigue Failure of Gas Turbines. Metals, 13, 701, DOI: 10.3390/met13040701

Gong, Yi., Ding, Q., Yang, Z-G. 2019. Failure analysis on premature fracture of anchor bolts in seawater booster pump of nuclear power plant. Engineering Failure Analysis, 97, 10-19, DOI: 10.1016/j.engfailanal.2018.12.008

Guma, T.N., Ozoekwe, N.C.W., Odita, K.V. 2020. An overview of approaches and techniques used in failure analysis of engineering system. Arid Zone Journal of Engineering, Technology and Environment, 16(3), 587-604.https://www.azojete.com.ng/index.php/azojete/article/view/343

Han, Y., Zhao, X., Bai, Z., Yin, C. 2014. Failure Analysis on Fracture of a S135 Drill Pipe. Procedia Materials Science, 3, 447 – 453, DOI: 10.1016/j.mspro.2014.06.075

Heinrich, M., 2022. Digital Twin Applications for Lifetime Extension of Heavy-Duty Mining Equipment. IEEE International Conference on Prognostics and Health Management (ICPHM), Detroit, MI, US (online).

Husaini, A.N., Putra, T.E., Novriandika, S. 2020. Study of Failure Analysis of a Fracture Crankshaft Pulley Used on a Truck Engine. IOP Conf. Series: Materials Science and Engineering, 739, 012018, DOI: 10.1088/1757-899X/739/1/012018

Ivković, D., Arsić, D., Cvetković, R.P., Popović, O., Nikolić, R.R., Bokuvka, O. (2023). How to replace the original material for the welded structure manufacturing. Production Engineering Archives, 29(4), 369–378. DOI: 10.30657/pea.2023.29.42

Katinić, M., Kozak, D., Gelo, I., Damjanović, D. 2019. Corrosion fatigue failure of steam turbine moving blades: A case study. Engineering Failure Analysis, 106, 104136, DOI: 10.1016/j.engfailanal.2019.08.002

Kaulgud, O.M., NangarePatil, B.H. 2016. Fracture analysis of machine components using fractography. International journal of advances in production and mechanical engineering, 2(2). https://www.academia.edu/87664132

Krishnakumar, K., Selvakumar, A. Metallurgical investigation of failure analysis in industrial machine components. 2020. Materials Today: Proceedings 27, 2076–2080, DOI: 10.1016/j.matpr.2019.09.071

Krynke, M., Ulewicz, R., Mielczarek, K. (2023). Determination of loads for load-bearing components in crane slewing mechanism considering their embedding stiffness. Transportation Research Procedia, 74, 608–615. DOI: 10.1016/j.trpro.2023.11.188

Lazić, V., Čukić, R., Aleksandrović, S., Milosavljević, D., Arsić, D., Nedeljković, B., Đorđević, M., 2014. Techno-economic justification of reparatory hard facing of various working parts of mechanical systems. Tribology in Industry 36(3) 287-292.

Maisuradze, M.V., Antakov, E.V. 2021. Analysis of Fatigue Failure Causes of Machine Components. Steel in Translation, 51(10), 745–751, DOI: 10.3103/S0967091221100089

Michałek, J., Tomek, L., Štalmach, O., 2019. Use of Fiber Bragg Gratings in the Monitoring of Load-Bearing Structures of Mining Machinery. IOP Conference Series: Materials Science and Engineering, 566(1), 012015.

Mohammed, M.N., Omar, M.Z., Zainuddin Sajuri, Salah, A., Abdelgnei, M.A. 2012. Failure analysis of a fractured connecting rod. Journal of Asian Scientific Research, 2(11), 737-741, https://archive.aessweb.com/index.php/5003/article/view/3422/5465

Mutavdžić, M., 2015. Modelling of the reparatory and manufacturing welding and hard-facing of the construction mechanization. PhD thesis, Faculty of Engineering, University of Kragujevac, Serbia 2015.

Pantazopoulos, G.A. 2019. A Short Review on Fracture Mechanisms of Mechanical Components Operated under Industrial Process Conditions: Fractographic Analysis and Selected Prevention Strategies, Metals, 9(2), 148. DOI: 10.3390/met9020148

Petrović, A., Momčilović, N., Sedmak, A., Đorđević, B, Dorin R., Milošević-Mitić, V., Bogojević, A., 2025. Reliability-based approach for structural integrity assessment of a bucket wheel excavator. Theoretical and Applied Fracture Mechanics, 136, 104849. http://dx.doi.org/10.2139/ssrn.4883522

Rocha Pinho, J.S., Contri Campanelli, L., Pereira Reis, D.A. 2022. Case study on the failure analysis of turbojet compressor blades, Tecnologia em Metalurgia, Materiais e Mineração/Metallurgy/Materials and Mining Technology, 19, e2760. http://dx.doi.org/10.4322/2176-1523.20222760

Sampath, S., Dhayalan, R., Kumar, A., Kishore, N.N., Sohn, H. 2021. Evaluation of material degradation using phased array ultrasonic technique with full matrix capture. Engineering Failure Analysis, 120, 105118. DOI: 10.1016/j.engfailanal.2020.105118

Savković, M., Gašić, M., Arsić, M., Petrović, R. 2011. Analysis of the axle fracture of the bucket wheel excavator. Engineering Failure Analysis, 18, 433-441. DOI: 10.1016/j.engfailanal.2010.09.031

Song, M.J.; Lee, K.H., Lee, J.-S., Kim, H., Kim, W.C., Lee, S.Y. 2025. Evaluation of Crack Formation in Heat Pipe-Welded Joints. Materials. 18(9), 2028. DOI: 10.3390/ma18092028

Sulaiman, S., Abidin Ismail, N. 2013. Analysis of failure in manufacturing machinery. IOP Conference Series: Materials Science and Engineering, 50, 012057. DOI: 10.1088/1757-899X/50/1/012057

Świt, G., Ulewicz, M., Pała, R., Adamczak-Bugno, A., Lipiec, S., Krampikowska, A., Dzioba, I. (2024). Innovative acoustic emission method for monitoring the quality and integrity of ferritic steel gas pipelines. Production Engineering Archives, 30(2), 233–240. DOI: 10.30657/pea. 2024.30.22

TAKRAF' SRs 1300.26/5.0+VR±10, Equipment manufacturer's documentation, Germany.

Vulovic, S., Zivkovic, M., Pavlovic, A., Vujanac, R., Topalovic, M., 2023. Strength Analysis of Eight-Wheel Bogie of Bucket Wheel Excavator, Metals, 13(3), 466, DOI: 10.3390/met13030466

Zangeneh, Sh., Ketabchi, M., Kalaki, A. 2014. Fracture failure analysis of AISI 304L stainless steel shaft. Engineering Failure Analysis, 36, 155-165, DOI: 10.1016/j.engfailanal.2013.09.013

Zhao, H., Wang, G., Wang, H., Bi, Q., Li, X., 2017. Fatigue life analysis of crawler chain link of excavator. Engineering Failure Analysis, 79, 737-748, DOI: 10.1016/j.engfailanal.2017.04.034.